Remote Sensing of Environment 159 (2015) 28–43

Contents lists available at ScienceDirect

Remote Sensing of Environment

journal homepage: www.elsevier.com/locate/rse

Eastern Europe's forest cover dynamics from 1985 to 2012 quantified from the full Landsat archive

P.V. Potapov [a,*], S.A. Turubanova [a], A. Tyukavina [a], A.M. Krylov [a], J.L. McCarty [b], V.C. Radeloff [c], M.C. Hansen [a]

[a] Department of Geographical Sciences, University of Maryland, College Park, MD 20742, USA
[b] Michigan Tech Research Institute, Ann Arbor, MI 48105, USA
[c] SILVIS Lab, Department of Forest and Wildlife Ecology, University of Wisconsin-Madison, Madison, WI 53706, USA

ARTICLE INFO

Article history:
Received 1 July 2014
Received in revised form 14 November 2014
Accepted 25 November 2014
Available online 30 December 2014

Keywords:
Landsat
Eastern Europe
Forest
Forest cover dynamics
Wildfires
Timber harvesting

ABSTRACT

In the former "Eastern Bloc" countries, there have been dramatic changes in forest disturbance and forest recovery rates since the collapse of the Soviet Union, due to the transition to open-market economies, and the recent economic crisis. Unfortunately though, Eastern European countries collected their forest statistics inconsistently, and their boundaries have changed, making it difficult to analyze forest dynamics over time. Our goal here was to consistently quantify forest cover change across Eastern Europe since the 1980s based on the Landsat image archive. We developed an algorithm to simultaneously process data from different Landsat platforms and sensors (TM and ETM+) to map annual forest cover loss and decadal forest cover gain. We processed 59,539 Landsat images for 527 footprints across Eastern Europe and European Russia. Our results were highly accurate, with gross forest loss producer's and user's accuracy of >88% and >89%, respectively, and gross forest gain producer's and user's accuracy of >75% and >91%, based on a sample of probability-based validation points. We found substantial changes in the forest cover of Eastern Europe. Net forest cover increased from 1985 to 2012 by 4.7% across the region, but decreased in Estonia and Latvia. Average annual gross forest cover loss was 0.41% of total forest cover area, with a statistically significant increase from 1985 to 2012. Timber harvesting was the main cause of forest loss, accompanied by some insect defoliation and forest conversion, while only 7.4% of the total forest cover loss was due to large-scale wildfires and windstorms. Overall, the countries of Eastern Europe experienced constant levels or declines in forest loss after the collapse of socialism in the late 1980s, but a pronounced increase in loss in the early 2000s. By the late 2000s, however, the global economic crisis coincided with reduced timber harvesting in most countries, except Poland, Czech Republic, Slovakia, and the Baltic states. Most forest disturbance did not result in a permanent forest loss during our study period. Indeed, forest generally recovered fast and only 12% of the areas of forest loss prior to 1995 had not yet recovered by 2012. Our results allow national and sub-national level analysis and are available on-line (http://glad.geog.umd.edu/europe/) to serve as a baseline for further analyses of forest dynamics and its drivers.

1. Introduction

European forests co-evolved with humans since the beginning of the Holocene, and their current distribution, structure, and dynamics represent a long history of clearing, alteration, and management (Fuchs, Herold, Verburg, & Clevers, 2013; Johann, 2004; Kalyakin et al., 2004; Kaplan, Krumhardt, & Zimmermann, 2009, 2012). Shaped by human activities, forests were a main sector of the economy providing food (e.g., hunting, livestock grazing, and plant products), timber products (e.g., lumber for construction and naval fleets, and pulp for paper), fuel (e.g., firewood, and charcoal), and other important resources (e.g., potash, and tar). The importance of forest resources, which can be quickly exhausted by unrestricted use, provided the impetus for forest mapping, inventory, and management. Forest mapping techniques were developed concomitantly with land tenure systems, and the first forest maps were already produced in the 14th century (Morse, 2007). In North and Central Europe, exhaustion of timber resources for naval ship building, lumber, and charcoal used for iron production, were the main factors why forest inventories were established in the 19th century (Eliasson, 2002; Tomppo, Gschwantner, Lawrence, & McRoberts, 2010). Forest inventories and management expanded into Eastern Europe and European Russia in the 19th and 20th centuries. In the 20th century, national forest inventory and monitoring incorporated various instrumental measurement methods, statistical sampling, and, later, remote sensing technology. As a result, the forests of Europe are among the most well-monitored ecosystems of the world.

Despite the wealth of forest inventory data, this information is unfortunately not readily available, nor well suited for region-wide analyses. One problem is that forest definitions and inventory methods

* Corresponding author.
E-mail address: potapov@umd.edu (P.V. Potapov).

http://dx.doi.org/10.1016/j.rse.2014.11.027
0034-4257/

vary among countries and have changed over time, making cross-national and multi-temporal comparisons complicated or even impossible (Seebach, Strobl, San Miguel-Ayanz, Gallego, & Bastrup-Birk, 2011). The lack of accessibility to national forest data poses another complication because many countries in Eastern Europe treat forest maps and precise forest statistics as either commercially sensitive or even a matter of national security, and thus prohibit its distribution beyond governmental agencies. Even where forest inventory information is in principle available, it is often hard to obtain from national (or sometimes regional) agencies where it is stored in a variety of formats.

Remote sensing (RS) data can provide an alternative data source to quantify forest cover and change independent of official governmental data sources. Information derived from satellite imagery, however, is not equivalent to inventory data collected by forest managers. Optical remote sensing data is suitable for mapping land-cover (tree canopy cover, dominant tree species composition) while national forest inventory data focuses on land-use (e.g., forest land). This means that while tree canopy cover change can be readily observed with remote sensing data, it is not directly comparable to harvested timber volumes reported by the national forest statistics. As a result, remote sensing data are rarely used as a primary source for national forest inventories, and statistical reports due to differences between land-use and land-cover forest definitions (Tomppo et al., 2010). The recent expansion in remote sensing-based forest monitoring products, however, highlights that these data could be valuable for many applications. First, remote sensing-based products can cover vast areas consistently, avoiding discontinuities due to administrative and national boundaries (Hansen et al., 2013; Kuemmerle, Radeloff, Perzanowski, & Hostert, 2006; Pekkarinen, Reithmaier, & Strobl, 2009; Potapov, Turubanova, & Hansen, 2011). Second, long-term records of satellite observations now available in image archives allow forest change quantification over several decades (Baumann et al., 2012; Griffiths, Muller, Kuemmerle, & Hostert, 2013; Margono et al., 2012; Potapov et al., 2012).

Spatial and temporal consistency is an inherent property of remote sensing-based forest cover and change products, alleviating the need for harmonization procedures commonly applied to regional and national forestry inventory data (Seebach et al., 2011; Tomppo et al., 2010). Simple biophysical criteria such as forest cover (defined using certain tree canopy cover thresholds without attribution to specific land cover categories and land use) make remote sensing-based products more suitable to assess carbon change than national forest inventories that are based on land use definitions (DeFries et al., 2002; Harris et al., 2012; Tyukavina et al., 2013). At the same time, remote sensing-based forest cover change analysis requires less effort and time than ground surveys, and can be performed in areas of limited ground access. This is why remote sensing-based products are widely used for multi-national forest assessments and change estimations, and their results serve as a baseline for carbon modeling and socio-economic analyses as well as for studies of landscape dynamics and biodiversity patterns (Burgess, Hansen, Olken, Potapov, & Sieber, 2012; Griffiths et al., 2012; Hansen et al., 2013; Harris et al., 2012; Kuemmerle, Hostert, Radeloff, Perzanowski, & Kruhlov, 2007; Tyukavina et al., 2013; Wendland et al., 2011).

While there have been prior assessments of forests in Europe with remote sensing (e.g., Gallaun et al., 2010; Pekkarinen et al., 2009; Schuck et al., 2003), none of them analyzed the full Landsat record for all of Eastern Europe. The lack of a comprehensive analysis of forest dynamics in Eastern Europe is unfortunate, because the region has witnessed numerous changes in forest cover since the collapse of socialism. Several remote sensing-based forest cover change projects have documented some of these changes (Baumann et al., 2012; European Environment Agency, 2007; Griffiths et al., 2013; Kuemmerle et al., 2009; Pekkarinen et al., 2009; Potapov et al., 2011). However, prior projects have several limitations precluding their use for analyses of forests dynamics across Eastern Europe: (i) none of these products cover the entire region; (ii) the methodologies used in different studies are not compatible; (iii) validation results are inconsistent and hard to compare; and (iv) with few exceptions (Potapov et al., 2011), products are not readily available.

Our research goal here was to fill these gaps and to produce a forest cover change product for all of Eastern Europe for nearly three decades using a consistent set of remote sensing data, methodology, and definitions. Our first objective was to develop a methodology that would allow multi-sensor data integration and seamless forest cover and change mapping. The methodology that we developed was then implemented to map forest cover change in Eastern Europe from 1985 to 2012. Our second objective was to provide consistent and rigorous validation of the reported forest cover change. Lastly, our third objective was the unrestricted sharing of the resulting product for further analyses (http://glad.geog.umd.edu/europe/). While we provide here an overview of the results and discuss potential forest change factors, the in-depth analysis of social and economic drivers of the observed forest changes was outside the scope of this project.

2. Data and methods

2.1. Study area

Our study area included the Eastern European countries that formed the "Eastern Bloc" until the end of the 1980s, except the former German Democratic Republic (aka East Germany, now part of Germany), and Albania (which disassociated from the Eastern Bloc in 1961). The study area included several former USSR republics (Estonia, Latvia, Lithuania, Belarus, and Ukraine) and the European part of Russia (Fig. 3A). The 2012 national and administrative boundaries of the countries were obtained from the Global Administrative Areas Dataset (GADM v2.0, http://www.gadm.org/). Because of the large variability in the hierarchy of administrative units as well as their size among the countries in our study area, we performed the sub-national analysis for administrative units only for the largest countries (Russia, Ukraine, Belarus, and Poland). For Romania and Bulgaria, we used the Eurostat territorial units for statistics (NUTS level 2, GISCO — Eurostat, European Commission; http://epp.eurostat.ec.europa.eu/) and the other countries were analyzed at the national level. To simplify area estimation, all data was processed in the Albers Equal Area projection with a spatial resolution of 30 m per pixel. The total study area encompassed 600 million ha, or 6.7 billion pixels.

2.2. Landsat imagery process

We analyzed Landsat Thematic Mapper and Enhanced Thematic Mapper Plus (TM/ETM+) imagery from the U.S. Geological Survey (USGS) Earth Resources Observation and Science (EROS) Data Center data archive. All imagery available in the USGS archives as off November 2013 were used for our project. In total, we processed 59,539 Landsat images, including 3436 from Landsat 4 TM, 26,400 from Landsat 5 TM, and 29,703 from Landsat 7 ETM+. The selected imagery dataset included all Level 1 Terrain corrected (L1T) growing season images from 1984 until the end of 2012 for the 527 Worldwide Reference System 2 (WRS-2) Path/Row scenes in our study area. We defined start and end of the growing season using Moderate Resolution Imaging Spectroradiometer (MODIS)-based 16-day Normalized Difference Vegetation Index (NDVI) profiles derived within MODIS-based forest cover mask for each Landsat footprint (Potapov et al., 2011). Consistent with our earlier research (Potapov et al., 2011), the growing season was defined as the sum of all 16-day intervals having an NDVI equal to or above 90% of the maximum annual NDVI.

All reflective bands (excluding ETM+ panchromatic band) of each Landsat image were converted to Top of Atmosphere (TOA) reflectance and the thermal band (high gain thermal band for ETM+) was converted to brightness temperature (Chander, Markham, & Helder, 2009). We did not conduct an atmospheric correction. A set of Quality Assessment (QA)

models were applied to each image yielding land, water, and snow/ice cover classes and probability of cloud, shadow, and haze contamination at per-pixel level. We developed the QA algorithm in our earlier work (Potapov et al., 2011), and improved it using additional input data. Each QA model consisted of a set of seven bagged classification trees (Breiman, 1996; Breiman, Friedman, Olshen, & Stone, 1984) derived from 193 training images distributed throughout the study area. We conducted a supervised classification for each training image to map land/water classes and cloud/shadow contaminated pixels. Based on initial results, we parameterized a separate set of QA models for TM and ETM+ sensors, and for scenes having a complete Shuttle Radar Topography Mission (SRTM) elevation data coverage (one of the inputs for the model; downloaded from CGIAR-CSI: http://srtm.csi.cgiar.org) and scenes outside SRTM coverage, where Global Multi-resolution Terrain Elevation Data 2010 (GMTED; Danielson & Gesch, 2011) were used. A total of 75 TM images (40 with SRTM and 35 with GMTED) and 118 ETM+ images (45 and 73 with SRTM and GMTED, respectively) were used to build four generic sets of QA models. Source data for the QA models included all image spectral bands, a cloud-free 2000–2012 median reflectance composite for the red, NIR and SWIR bands (Hansen et al., 2013), and Digital Elevation Model (DEM)-based variables. The DEM-based variables included elevation, slope, aspect with respect to actual sun position, and illumination (Richter, 2010). Our shadow detection model used distance to detected clouds calculated using acquisition sun azimuth. After we implemented the QA mask, each pixel was classified as either clear-sky land, water, ice, or cloud/shadow contaminated. To exclude pixels affected by light scattering from neighboring clouds, a two-pixel area around clouds was also mapped as a separate QA state.

After the QA screening, we applied a normalization and a surface anisotropy correction using global Top of Canopy (TOC) reflectance from MODIS as reference. The relative normalization to the common reflectance target (MODIS data) was applied to ensure consistency between sensors in time and space. We used the MOD44C (collection 5) standard product, which consists of 16-day composites of reflective and thermal bands after atmospheric correction (Vermote, Saleous, & Justice, 2002; Carroll et al., 2010) from 2000 to 2010 to compile a global seamless cloud-free TOC reflectance dataset for red, NIR, and two SWIR MODIS bands (Potapov et al., 2012). For each Landsat image, we created a Pseudo-Invariant Objects Mask (PIOM) automatically. First, we excluded all detected cloud/shadow contaminated pixels and water from PIOM. Second, we excluded pixels with >5% difference in reflectance between MODIS TOC and Landsat TOA. We computed the spectral reflectance difference for Landsat red, NIR and SWIR (bands 5 and 7) and corresponding MODIS bands for all pixels within the PIOM, and modeled the reflectance bias as a function of the Landsat scan angle (Hansen et al., 2008; Potapov et al., 2012). When we applied the derived model to every pixel in the Landsat images, it resulted in normalized, anisotropy-adjusted reflectance values. Shortwave Landsat spectral bands (blue and green) were not normalized and not used for further processing. Surface brightness temperature was used without normalization. We also computed the NDVI and Normalized Difference Water Index (NDWI; Gao, 1996) for every image as additional data layers.

2.3. Landsat time series and multi-temporal metrics

The Landsat imagery process resulted in a time-series of cloud- and shadow-free normalized reflectance observations. From this time-series, we derived a suite of multi-temporal metric sets for each 30-m pixel, each metric set for a specific purpose (Fig. 1). Multi-temporal metrics are useful transformations of image time-series for both coarse resolution (DeFries, Hansen, & Townshend, 1995; Hansen, Townshend, DeFries, & Carroll, 2005; Reed et al., 1994) and medium resolution data (Broich et al., 2011; Hansen et al., 2013; Potapov et al., 2012), and facilitate land cover and land cover change mapping and characterization both the state of biophysical variables such as biomass and height (Pflugmacher, Cohen, & Kennedy, 2012) and the change in biomass

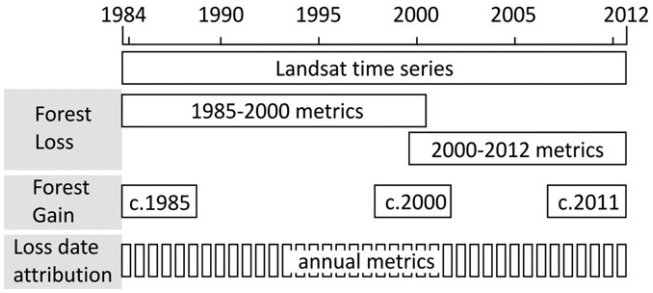

Fig. 1. Landsat time series and multi-temporal metric sets.

over time (Pflugmacher, Cohen, Kennedy, & Yang, 2014). For gross forest cover loss mapping, we derived two "long interval" metric sets: one for 1985–2000, and a second for 2000–2012, identical to the recently published global forest loss product (Hansen et al., 2013). These metric sets had a 1-year overlap to insure that change around year 2000 was correctly detected. To map tree canopy cover and ultimately forest cover gain, we derived a 3-year "short interval" metric set for circa year 1985 (1984–1986), 2000 (1999–2001), and 2011 (2009–2012). In addition, a set of annual metrics were produced to compliment longer interval datasets and to assign the date of gross forest cover loss events.

The "long interval" metric sets (1985–2000 and 2000–2012) were constructed from all cloud-free observations between the last available observation before the start of the first year (1985 or 2000) and the last available observation of the last year (2000 or 2012). The mean start and end dates of the observations that we included were 26 April 1985 and 5 August 2000 for the 1985–2000 interval, 13 October 1999 and 8 August 2012 for the 2000–2012 interval. The average number of cloud-free observations used to calculate metrics was 30 per pixel for the 1985–2000 interval and 70 for the 2000–2012 interval.

To calculate the multi-temporal metrics, we implemented two main approaches: one based on time-sequential reflectance change, and another based on reflectance ranking (Table 1). For the first approach, we analyzed the spectral reflectance time-series and corresponding observation dates. For the second approach, we ranked the spectral band reflectance from low to high (each band was processed individually), or ranked observations by the corresponding NDVI, NDWI, and brightness temperature ranks. In addition to metrics based on individual

Table 1
Multi-temporal metrics derived from Landsat time-series.

Metrics extracted from observations ordered by date
Computed independently for each Landsat spectral band (3, 4, 5, and 7), NDVI and NDWI
First and last cloud-free observation
Median and mean of three earliest and latest observations
Slope of linear regression between reflectance value and observation date
Difference between maximal value and preceding/following minimal values
Difference between minimal value and preceding/following maximal values
Largest reflectance drop or gain between consecutive observations
Metrics extracted from observations ranked by band (index) value
Computed independently for each Landsat spectral band (3, 4, 5, and 7), NDVI and NDWI
Reflectance (index) value corresponding to selected rank (minimum, 10%, 25%, 50%, 75%, and 90% percentiles, maximum)
"Symmetrical" averages for all values between selected ranks (minimum–maximum, 10%–90%, 25%–75%)
"Asymmetrical" average for all values between selected ranks (minimum–10%, 10%–25%, 25%–50%, 50%–75%, 75%–90%, 90%–maximum)
Metrics extracted from observations ranked by corresponding NDVI, NDWI, or brightness temperature
Computed for each Landsat spectral band (3, 4, 5, and 7)
Reflectance value corresponding to selected rank (minimum, 10%, 25%, 50%, 75%, and 90% percentiles, maximum)
"Asymmetrical" average for all values between selected ranks (minimum–10%, 10%–25%, 25%–50%, 50%–75%, 75%–90%, 90%–maximum)

observations, we used annual median reflectance values to calculate first and last year metrics and the slope of linear regression of the annual median reflectance as a function of the year of observation.

The 3-year metric centered on years 1985, 2000, and 2011 included only observations for the center year plus one year before and after. If no cloud-free observations were available during these years, then we expanded the search interval to ±2 years of the target date. The 3-year metric sets were based only on reflectance ranking (selected percentiles, "symmetrical" and "asymmetrical" averages). The annual metric set was based only on observations within a single calendar year (if no observations were found, metric value was defaulted to "no data"), and included minimal, maximal, and median spectral band reflectance, NDVI, and NDWI values within the year.

2.4. Forest cover change mapping

We defined gross forest cover loss ("forest loss" hereafter) as any disturbance event, be it a natural disturbance or a human disturbance such as logging, resulting in complete or nearly complete tree removal in a given 30-m Landsat pixel. Based on this definition, we treated forest loss within natural, managed forests and tree plantations the same way. Classifications were implemented at per-Landsat pixel level, with a minimum mapping unit equivalent to 0.09 ha. We mapped forest loss as a single dynamic class using a supervised bagged classification tree algorithm (Breiman, 1996; Breiman et al., 1984). To balance between model stability and computation time we employed seven classification trees in the bagged tree model. Training areas for 1985–2000 were collected using visual interpretation of the first and last dates, and maximum reflectance composites. We added training data iteratively until we achieved the desired quality of the output map. In total, the manually selected training polygons of forest loss and forest persistence included 21 million pixels. For each classification iteration, we sampled randomly 20% of source training data seven times to build seven bagged classification trees. Training data served as the dependent variable and the 1985–2000 time interval metrics as the independent variable in the tree model. We applied our classification trees to the entire study area yielding a forest loss map. For 2000–2012, a forest loss map was already available as part of a global forest change assessment (Hansen et al., 2013). However, the global classification model was a conservative estimate of forest loss, and thus had higher forest loss omission rates than our 1985–2000 model. To improve product accuracy and consistency across the entire time series, we performed a new regional change classification for 2000–2012 using results of the global change mapping as training data. Seven bagged classification trees were created using 0.1% sampling of no-change areas and 0.5% sampling of change areas from the global product as dependent variable and 2000–2012 metrics as independent variables (3.5 million training pixels per tree model in total).

While forest cover loss usually results in a clear and immediate change in spectral reflectance, gain of forest cover is a gradual process with subtle annual change of spectral properties. We define gross forest cover gain ("forest gain" hereafter) as areas where tree canopy cover reached a certain threshold by the end of our study period. Instead of mapping forest gain using a single classification model, as we did when mapping forest loss, we decided to use a post-classification comparison of the tree canopy cover maps for circa 1985, 2000, and 2011, which were produced using 3-year metric sets. The use of annual tree canopy cover maps was not viable due to the data gaps and low tree canopy cover model stability in "data poor" years and regions. We created a bagged regression tree model using circa-2000 (1999–2001) metric set and tree canopy cover training data from the global year 2000 product (Hansen et al., 2013). The global product, however, overestimated tree canopy cover within peat bog areas in the northern part of our study area. To address this problem, we manually added training sites where the initial tree canopy cover results were incorrect. A set of seven bagged regression trees were created incorporating 0.1% random sample from global tree canopy cover product and manually created training as dependent variables (3.5 million training pixels per tree). The same regression tree model was implemented for all three dates to insure consistent tree canopy cover mapping. To map areas that changed in land cover from non-forest to forest during analyzed time interval, we had to define "forest cover" using a tree canopy cover threshold. A simple comparison of aggregated areas under canopy cover classes with official forest area for each country (FAO, 2010) and each Russian region (ROSLESINFORG, 2003) did not result in a single consistent threshold. Instead, we used a previously published Landsat-derived forest cover map for European Russia (Potapov et al., 2011). The threshold of >=49% tree canopy cover resulted in the same forest area as in the previously published map, and we used this threshold to define persistent forest cover and to map forest gain from 1985 to 2012. Forest loss pixels were classified as "no forest gain", "forest cover established by year 2000", and "forest cover established by year 2012". Mapping forest gain within areas that had no forest cover in 1985 was based on a post-classification comparison of tree canopy cover for 1985, 2000, and 2012. Initial results based on a simple comparison showed that sub-pixel image misregistration caused some false forest gain along edges of forests. To remove these false changes, we increased the minimum mapping unit for forest gain from a single Landsat pixel (0.09 ha) to 0.45 ha, and removed all forest gain areas below this threshold.

2.5. Forest cover change date attribution

We assigned the date for each forest loss event based on the time series of two annual products: minimum annual NDVI (within growing season) and annual tree canopy cover. The first product was part of the annual multi-temporal metric set, and annual tree canopy cover was mapped using a separate bagged regression tree model. We used stable forest areas in the circa year 2000 tree canopy cover product to select 0.1% of the study area as training data, and annual metrics from years where sufficient cloud-free data coverage existed (1986–1989, 1994, and every second year after 2000) as independent variables to create the generalized tree model. The resulting tree model was applied annually. At the pixel level, only pixels with at least one cloud-free observation within the year were processed, otherwise the pixel was marked as "no data" for the given year. We then analyzed both tree canopy cover and the minimum annual NDVI time series for each forest loss pixel, and applied a set of heuristics to assign forest loss date with high, medium or low certainty level. If a pixel had a tree canopy cover above 49% for at least two successive years, and then tree canopy cover dropped below 20% and did not increase for at least one year, then loss event date was assigned with the high certainty. More than 52% of all forest loss pixels had this high level of certainty. However, if no high certainty sequence was found, then the year with the highest tree canopy cover drop was assigned as the loss date with a medium level of certainty. If the tree canopy cover trend analysis did not produce any results (1.4% of all loss pixels), then we used the date of the highest NDVI drop instead, and assigned a low detection certainty. For pixels where the loss date was assigned with low certainty, especially in the case of mixed-pixels on the boundary of loss areas, the loss date may be assigned incorrectly. To fix these problems, we applied a 90-m radius moving window filter for pixels where the loss date was detected with low or medium certainty, and assigned it as the majority of the loss date for pixels in the neighborhood. This filtering process had the effect of improving date assignments for edge or mixed pixels that were labeled differently to adjacent pure change pixels. The majority filter altered the loss date for less than 10% of all forest loss pixels. In relatively rare cases, a second loss event was assigned for a pixel. This occurred when a pixel was mapped as forest loss during both time periods, 1985–2000 and 2000–2012. However, a second loss date was assigned only if both first and second date were assigned with the highest certainty.

Because the annual tree canopy cover products had temporal gaps due to clouds and inconsistent data acquisition, the date of forest loss detection was not always preceded by a year with cloud-free data. To account for this effect, we recorded the number of years between a loss event and the preceding cloud-free observation for each change pixel and used it to allocate change area over time (see Section 3 below).

To analyze the annual trends of forest loss we performed a linear regression model fit of the annual forest loss time-series. The slope of linear regression between y = annual loss versus x = year was derived using linear least squares method. The p-value of the slope per regression model was used to measure significance of the forest loss trend within countries and regions.

For forest cover gain, it is not meaningful to assign a specific year as the year when the gain occurred, especially in boreal and temperate forests where tree canopy cover and tree height gradually increase as trees grow on previously open land. Instead, we assigned dates only for 2000 or 2012, i.e., the years where we mapped tree canopy cover using the 3-year metrics. This resulted in two nominal periods for quantification of forest gain, 1985–2000 and 2000–2012.

2.6. Thematic attribution of forest cover loss and gain

Forest loss can occur due to a range of causes, and we separated forest loss due to large wildfires and windstorms from all other types of disturbance (including logging, conversion, and disease). The analysis was based on visual interpretation and manual delineation of large-scale natural disturbance. Only large disturbance areas (>20 ha) that were unambiguously either fire or wind-damage were mapped. Smaller natural disturbances and areas where wind-damage was immediately followed by salvage logging were left in the "other" disturbance type category.

In terms of forest gain in areas that were non-forest in 1985, we separated reforestation, defined as forest gain after forest disturbance (be it natural or due to harvesting) from afforestation, defined as forest cover gain within abandoned agriculture lands. First, we applied a supervised decision tree classification using 0.5 million training pixels manually mapped as agriculture or other non-forest category in the year 1985. The classification was complemented by extensive manual correction of the resulting classification using visual interpretation of 1985 land-use within the forest-gain mask. This correction step was especially important in the southern part of the region where spectral signature of tilled agricultural areas and recent clear-cuts were very close. Visual interpretation allowed us to employ other criteria, such as the location and shape of the forest gain patch, to correctly map 1985 land-use.

2.7. Forest dynamics types

After compiling the forest loss and forest gain maps with the forest cover extent for the year 1985 (defined using >=49% TCC threshold), we produced a map of forest dynamics types (Fig. 2). We defined basic types of forest dynamics to support further analysis and to generate summary statistics. Dynamics types A and B were stable non-forest and forest, where we detected no change events. Types C and G were areas where forest cover gain occurred from non-forest in 1985. The difference between these two types is that the second type (G) experienced forest cover loss after forest cover gain. Types D, E, and F represent forest cover loss. Forest gain occurred after loss in areas of types E and F, and with a second loss event mapped for type F. In type D we did not observe forest gain after loss, either due to a short time interval between the loss event and the end of study period (2012), or because of permanent forest clearing (in case of agriculture, settlement, or infrastructure expansion). Figs. 3 and 4 illustrate Landsat image composites and classification results: forest dynamics types and the dates of forest loss.

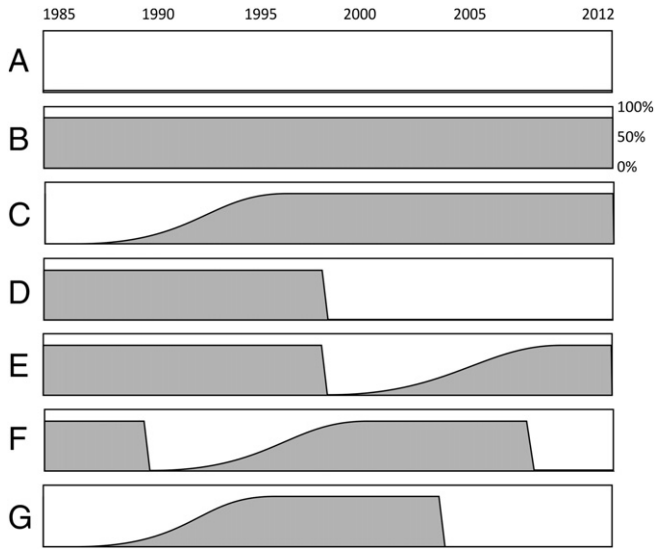

Fig. 2. Forest dynamics types. Scale on the right represent tree canopy cover. A — Stable non-forest; B — stable forest; C — forest gain over non-forest in 1985; D — forest loss; E — forest loss followed by forest gain; F — repeated forest loss separated by forest gain; G — forest loss on areas which gain forest cover after non-forest state in 1985.

2.8. Validation

We validated the accuracy of our forest loss and forest gain maps using a probability-based stratified sample of individual 30-m pixels. The sampling design followed Stehman (2012) and Tyukavina et al. (2013), the accuracy assessment was performed according to Stehman and Czaplewski (1998) and Olofsson et al. (2014), and the sample-based area estimation was performed according to Stehman (2013). The sampling and validation were done separately for forest loss mapped for 1985–2000 and 2000–2012 to compare the accuracy of the two analyses. We selected strata based on the assumption that most of the commission and omission errors are tied to change area boundaries (see Tyukavina et al., 2013). We identified a one-pixel buffer outside and inside change areas as "peripheral no change" and "peripheral loss", and the remaining pixels were assigned to "core loss" and "core no change" strata. The "peripheral" strata were designed to target likely areas of change omission and commission error.

We validated areas of forest gain within 1985 forest (that was subsequently lost) and 1985 non-forest areas separately. In addition, we defined strata specifically to validate accuracy of land-use change mapping (reforestation on forest land-use lands vs. afforestation of agriculture lands). The sample design (total number of pixels within study area and number of samples) is presented in Table 2.

The total number of samples was selected to balance anticipated standard error and available resources for image interpretation: 1000 for each of forest loss classifications and 500 for each of forest gain classifications. Sample allocation for the forest loss validation was a compromise between equal and proportional: more samples were allocated to the "peripheral" strata where the majority of misclassified map pixels were anticipated to be found. In the case of forest gain within 1985 non-forest areas we also employed an intermediate allocation between equal and proportional to target relatively rare forest gain classes. Proportional allocation was used for forest gain following forest loss where strata areas were comparable. We did not conduct a validation of the forest loss thematic attribution (windstorms and wildfires) because this product was based on visual interpretation of clearly defined patterns on Landsat imagery, and no independent validation data was available.

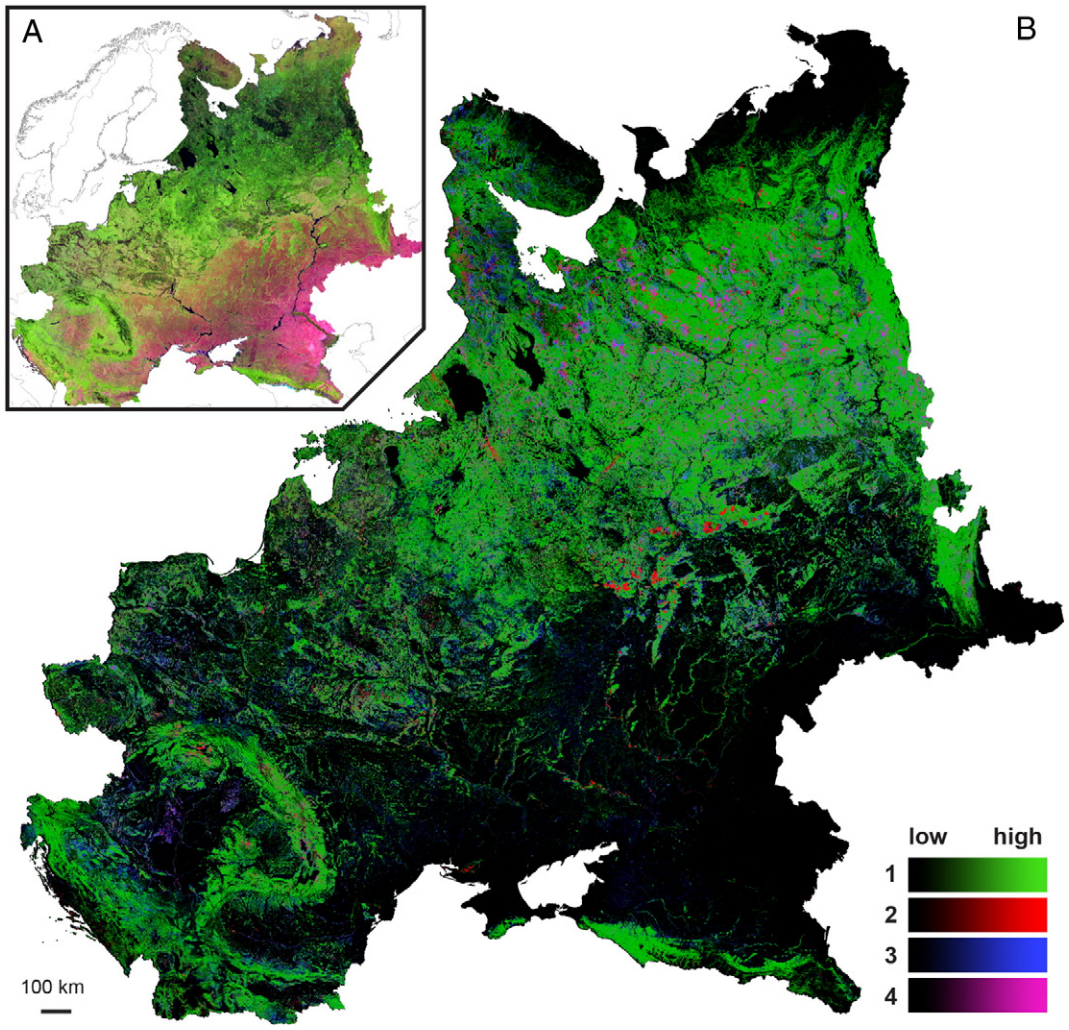

Fig. 3. A. Circa year 1985 Landsat image composite for the entire region of analysis (SWIR-NIR-red RGB band combination). Areas outside region of analysis shown in white. B. A color composite of stable forest cover in green (1), gross forest cover loss in red (2), and gross forest cover gain in blue (3). Magenta (4) represent areas with forest cover loss followed by forest gain. For visualization purposes, we resampled the dataset to a 300-m pixel grid, and calculated the percentage of the pixel area with forest cover and forest change values. For the visualization, each layer scaled independently to highlight geographic pattern of forest dynamics.

The only reference data available to collect information for our validation sample for 1985 to 2012 were Landsat imagery. High spatial resolution imagery data over the study period are largely non-existent, and only available since 2000. We decided against using different sources of reference data for the 1985–2000 and the 2000–2012 accuracy assessment, because this would make the validation results incompatible. To create a consistent sample validation dataset, we complied annual Landsat composites. All available annual median composites, together with selected annual metrics and products, were visually examined for every validation sample (Fig. 5). Our Landsat-based per-pixel visual change detection method is similar to the TimeSync application developed by Cohen, Yang, and Kennedy (2010) to assess the accuracy of Landsat-derived forest change products. Sample pixels were interpreted by a regional forest mapping specialist (S.T.), and ambiguous samples were cross-validated by a second observer (A.T. or P.P.). Validation results were used to report model accuracy measures and associated confidence intervals following Olofsson et al. (2014). Sample-based class areas were computed from error matrices using a stratified estimator (Stehman, 2013).

We also conducted a limited field verification of our forest gain map focusing on abandoned agriculture areas in several regions of European Russia (Kirov, Nizhny Novgorod and Vladimir) during the summers of 2012 and 2013. We selected these regions because they had extensive forest gain on former agriculture lands. Conducting field work throughout our entire study area was unfortunately beyond the scope of our project. In total, we collected 75 field points within different stages of abandonment and afforestation. Point samples were randomly selected within abandoned areas. For each point we visually assessed tree canopy cover and measured tree canopy height using a clinometer. For 58 points we also measured the age of the oldest trees found within the abandoned area with an increment borer.

3. Results

The forest cover for year 1985 (sum of dynamics types B, D, E, F, see Fig. 2 for explanation) was 216 million ha (Table 3). By 2012, forest area increased by 10 million ha (4.7%) and reached 226 million ha (sum of types B, C, E). In total, there were 24 million ha of forest loss (including areas that experienced forest gain after loss), which was substantially lower than the 34 million ha of forest gain. Forest loss of 1985 forests (sum of types D, E, F) represented 11% of the 1985 forest area, or 0.41% of forest loss/year. The majority (58%) of the forest loss areas were reforested by 2012. Indeed, by 2012, more than 15% of the total forest area consisted of young forests originating within the previous 27 years. Forest gain on 1985 non-forest lands represented 5.8% of the 1985 non-forest land area (excluding permanent water). Forest dynamics types

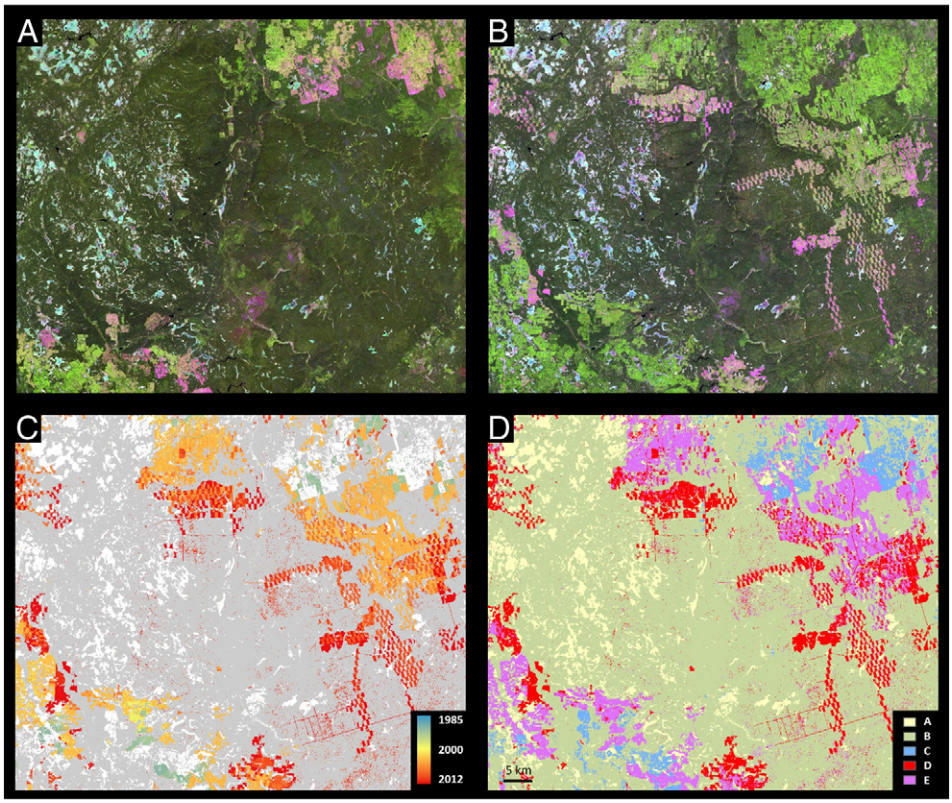

Fig. 4. (A) and (B) — Landsat image composites for years 1985 and 2012, respectively (SWIR-NIR-red RGB band combination). (C) — Annual gross forest cover loss (stable forest cover shown in gray). (D) — Forest dynamic types (see Fig. 2 for the definitions of the types. Forest dynamics types F and G were generally rare and not present within the subset). Area centered on 43°19′E 63°27′N (Russia, Arkhangelsk region). Within the subset, forest loss areas include clear-cut logging (large blocks), logging for infrastructure development (linear features), and bark beetle damage (scattered small-scale loss events).

that experienced a second loss event (F), as well as forest loss within forest gain areas established over 1985 non-forest lands (G) were rare, and generally reflective of specific land dynamics (e.g., we found type G mostly within year 2010 burned areas in Russia, where fires affected forests of all age groups).

The attribution of year to each forest loss event (Fig. 6) was affected by the lack of cloud-free observations in some years (Fig. 10). When we examined the assigned date by itself (Fig. 6, a), then the annual change area has high variance among years, especially during 1989–1998, which was a period of low Landsat data availability in the USGS archive.

Table 2
Stratified sampling design for gross forest cover loss and gross forest cover gain validation.

Strata	Total number of pixels	Samples (30 m pixels)
Gross forest cover loss 1985–2000		
Core loss	51,008,874	110
Peripheral loss	85,499,238	130
Peripheral no change	156,547,255	160
No change	6,378,510,240	600
Gross forest cover loss 2000–2012		
Core loss	43,090,561	110
Peripheral loss	87,088,209	130
Peripheral no change	149,958,610	160
No change	6,391,428,227	600
Gross forest cover gain within gross forest cover loss		
No change	113,044,410	210
Forest gain	153,642,472	290
Gross forest cover gain within non-forest areas of 1985		
Reforestation (over logging/fires)	153,409,335	136
Afforestation (over ag lands)	71,544,209	64
No change (stable non-forest)	4,047,459,920	300

The majority of the forest loss was accordingly attributed to years 1999 or 2000, which is when Landsat 7 became operable. To reduce the impact of image acquisition gaps, we allocated the change detected in a given year equally over the time interval between the detection year and the year with the last cloud-free observation before the change detection (Fig. 6, b). This approach resulted in markedly different annual forest loss totals during the decade with low image availability (1988–1998).

The aforementioned allocation of change area, however, did not fully suppress the disproportionally large change detected in year 2000, principally due to pre-2000 data gaps that precluded the appropriate annual assignment of forest cover loss. To further reduce the effect of data gaps, we calculated average annual change area for multi-year intervals (1986–1988, 1989–2000, 2001–2006, 2007–2012). Comparison of these intervals for the entire study area (Fig. 6, d) showed that the annual forest loss decreased during the 1990s by 26% compared to 1986–1988, and increased since the early 2000s, with average annual loss from 2007 to 2012 22% higher than that in the 1986–1988 time interval. To validate this general trend, we calculated the annual change area for only those pixels for which the change date was allocated with the highest certainty (Fig. 6, c). For these pixels, the number of available acquisitions did not affect the loss date assignment, because they represent only pixels with the strictest change date assignment criteria. The trends in annual forest loss for these pixels were very similarly to those for the interval averages for all pixels (Fig. 6, d), including the decrease in the 1990s and increase in the 2000s.

Of the total forest loss area, we attributed 1.3% to windfalls and 6.1% to wildfires. The area attributed to these disturbance types increased toward the end of the time period (Fig. 7). The upward trend was statistically significant for both wildfires ($p < 0.015$) and windstorms

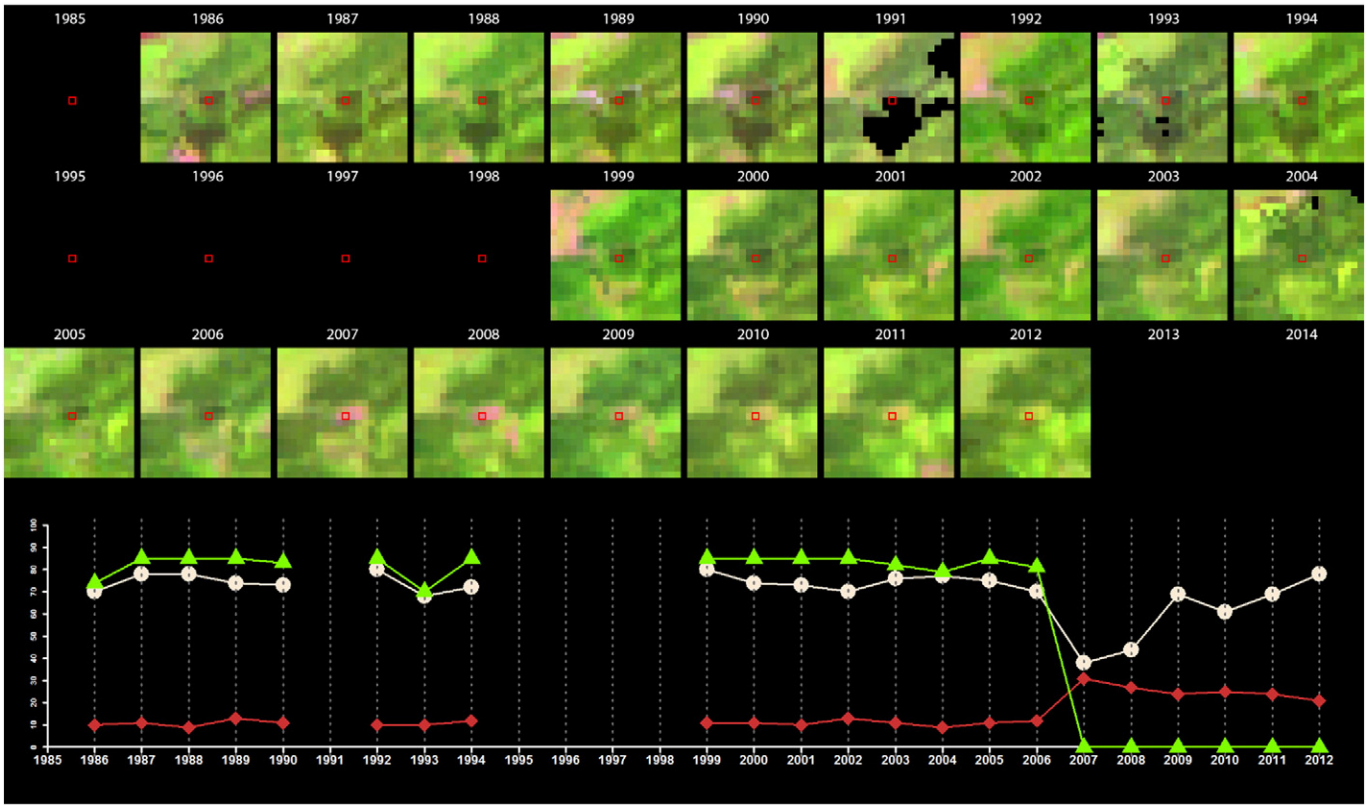

Fig. 5. Validation data used for validation pixel interpretation. Upper part — available Landsat image composites (band combination SWIR-NIR-red). Cloud or shadow contaminated pixels were removed. The sample pixel is outlined in red (location 24.4101 E, 55.1556 N). The graph at the bottom shows annual profiles of SWIR band reflectance (red line), tree canopy cover (green line) and minimum NDVI (white line) for this sample pixel. In this example, forest loss occurred in 2007 without subsequent forest gain. Visualization images were automatically prepared for all validation pixels using GDAL and R software packages.

($p < 0.001$). Forest loss due to wildfire was often detected with a one-year lag though due to cloud and smoke contamination during the fire year, which reduced image availability, and also because fires sometimes occurred after the last cloud-free Landsat acquisition for the fire year. During an extreme fire year, large proportions of the total forest loss may be due to fire. For example, in 2011, 29% of all forest loss was due to wildfires. In comparison, windstorm damage did not contribute more than 7% of total forest loss even during extreme years.

While forest loss was widespread, forest generally recovered fast (Fig. 8). More than 60% of the total area where forest loss occurred prior to 2007 had a tree canopy cover above 49% by 2012, and this rate was more than 85% for pre-1988 loss areas. The highest rate of forest recovery occurred in European Russia (where forest loss rates were highest in the 1980s) and the lowest in Macedonia, potentially due to dry climate conditions slowing tree regrowth.

The total forest gain on areas that were not forests in 1985 was over 20 million ha. Of this area, 68% (or 13.6 million ha) was due to forest land-use dynamics (reforestation after pre-1985 forest loss), and 32% (or 6.4 million ha) due to forest growth on former agricultural land. The reforestation of forest disturbance happened largely before 2000 (72% were reforested by this date), while afforestation of former agricultural lands occurred largely between 2000 and 2012 (53% of the total afforestation area).

The trends of forest cover change and forest loss area at the national level for the 20 countries in our study area were highly variable and illustrated the diversity of forest land change dynamics in Eastern Europe (Table 4). Forest cover area increased in all countries except Estonia, Latvia, and Macedonia. Annual forest loss trends varied substantially among countries, and among epochs: 1986–1988 (socialism), 1989–2000 (transition and post-socialism), 2001–2006 (before economic crisis), and 2007–2012 (during and after economic crisis). These differences are discussed below in Section 4.3.

Across Eastern Europe, there were pronounced regional hotspots of forest loss rates (Fig. 9A), and changes in annual forest cover loss area (Fig. 9B), as well as of net forest cover area change (Fig. 9C), and forest gain on former agricultural areas (Fig. 9D). Differences in these metrics were pronounced among counties, and there was substantial variability among administrative regions within Russia, Ukraine, and Poland.

Table 3
Area of forest dynamics types 1985–2012.

	Forest dynamics type	1985 forest cover	2012 forest cover	Area, ha * 1000
	No data			0.5
A	Non-forest (stable)	N	N	364,272
B	Forest (stable)	Y	Y	192,056
C	Forest gain on 1985 non-forest	N	Y	20,111
D	Forest loss	Y	N	9974
E	Forest loss followed by forest gain	Y	Y	13,828
F	Forest loss followed by forest gain, and another forest loss (two loss events)	Y	N	64
G	Forest gain on over 1985 non-forest followed by forest loss	N	N	135

The "no data" areas represent several small Croatian islands that are outside the Landsat processing area.

3.1. Validation results

Our sample-based estimated accuracy assessment (Table 5) showed reliable classification model performance for both forest loss and forest gain classifications. The expert-driven model (forest loss 1985–2000)

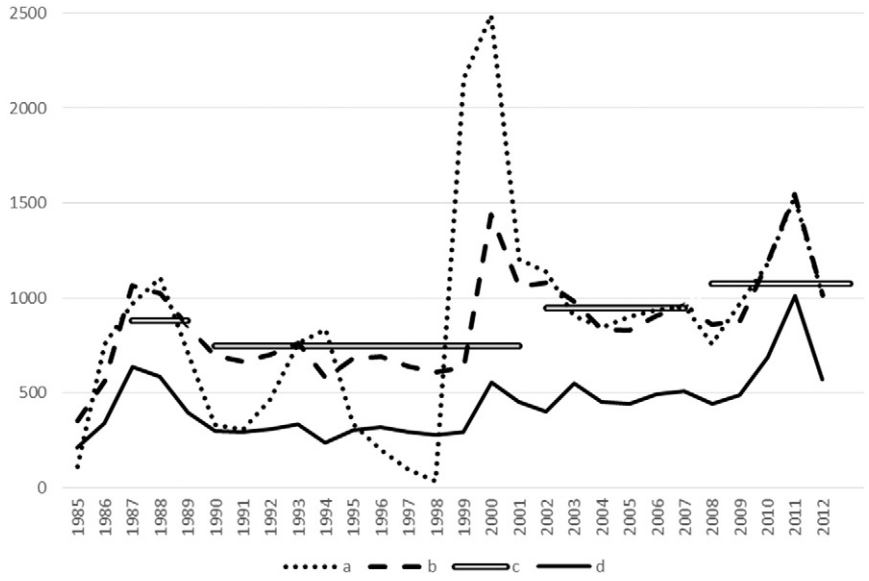

Fig. 6. Annual gross forest cover loss area (ha * 1000). (a) Area by date of change detection; (b) area of change distributed over years between detection and the last cloud-free observation; (c) average annual change area for intervals 1986–1988, 1989–2000, 2001–2006, 2007–2012; (d) area of change allocated with the highest certainty distributed over years between detection and the last cloud-free observation.

delivered balanced omission and commission errors, which was the objective of our iterative classification approach. The forest loss 2000–2012 model based on existing training resulted in a higher omission rate, and hence a 6.96% difference between map-based and sample-based area estimate. The high accuracy of forest gain after forest loss can be explained by relative simplicity of the change event and small total area of both classes (limited by forest loss). The forest gain detection within 1985 non-forest areas had the lowest accuracy of all of our results. The comparison of sample-based and map-based estimates showed that the post-classification approach that we employed for the change detection failed to map 21% of the forest gain area.

The accuracy of the attribution of forest gain to either preceding forest loss or agricultural land-use was assessed only for those pixels that were correctly mapped as afforestation (182 samples). In total, 83.52% of those samples were allocated to the correct classes. The majority of expert-interpreted forestry land-use samples were mapped correctly (94.44%), while a substantial percent of agriculture land-use pixels (32.43%) were falsely attributed as forestry land-use. Thus, the area of afforestation on former agricultural lands was possibly underestimated.

Our validation of the forest loss date allocation was based on a sample of 887 forest loss pixels from forest loss 1985–2000, forest loss 2000–2012, and forest gain after forest loss sample sets, where we could interpret the reference date unambiguously. It should be noted that analyst can interpret the date of change event only from available Landsat acquisitions, and so this date may not represent the actual forest loss date but the date of the first clear Landsat image after the change event. For each sample, the date assigned by the automatic model was compared to date assigned by visual interpretation of annual image composites. The date was correctly determined for 76.4% of samples; and 89.9% of samples had a date difference of ± 1 year. On average, the allocation model assigned the date of forest loss of 0.26 years later compared to actual change event date. Pixels for which the date was assigned with the highest certainty had the lowest average difference compared to the actual change event (0.17 years later). The highest difference in date (almost 3 years on average) occurred in the case of samples with the

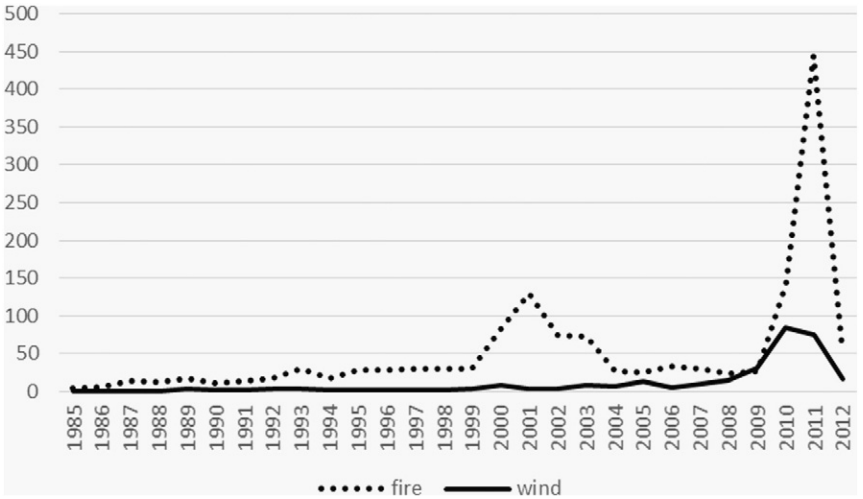

Fig. 7. Annual area (in ha * 1000) of gross forest cover loss attributed to windstorms and wildfires.

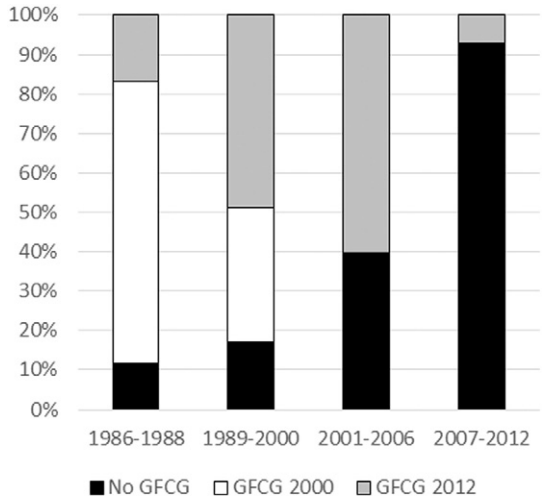

Fig. 8. Percent forest gain within forest loss areas as a function of the year of the forest loss.

lowest certainty of the date allocation (i.e., where NDVI time-series was used instead of tree canopy cover annual data).

Field verification results (Table 6) confirmed that our tree canopy cover threshold resulted in an accurate forest gain detection. The majority of plots with more than 50% tree canopy cover in the field were correctly mapped as forest gain. For broadleaf and pine tree forests growing on abandoned lands in the central part of European Russia this threshold corresponded to a median tree height above 6 m and an age older than 12 years. Our field-based results, however, are only valid for regrowth on abandoned agriculture areas in the hemiboreal forest zone.

4. Discussion

4.1. Data availability

The USGS Landsat program is the oldest provider of operational medium-resolution satellite data. The data record of Landsat TM/ETM+/OLI instruments spans over last 30 years, and the free data access and redistribution policy made it the best data source for the analysis of long time-series of land cover change. The main problem of the existing archive, however, is an inconsistent data acquisition record. A dramatic decline in acquisitions occurred after the commercialization of the Landsat 5 satellite in 1984, with a considerable amount of data collected by international ground receiving stations. While data from international ground receiving stations are currently being transferred to the USGS EROS archive, the degree to which they may fill the existing data gap over Eastern Europe was unclear when we conducted our study. Another factor reducing data availability are problems with Landsat 4 and 5 imagery calibration precluding the conversion to terrain corrected L1T data. Together, these limitations cause low image availability before 1986 and between 1989 and 1998 (Fig. 10). This is unfortunate, because the number of growing season images per footprint determines the amount of cloud-free data available within the study area. A nearly 100% annual cloud-free coverage is available only during years for which there are seven or more images per footprint. However, such a high number of acquisitions cannot be obtained by a single sensor for the entire region. The growing season length (as defined using MODIS data, see Section 2.2) is highly variable across the study area, but only 80 days in tundra regions, 110 days in the temperate part of the study area, and 160 days in the south. A single Landsat sensor with an observation frequency once per 16 days will acquire only 5 images in the tundra region, and less than 7 in the temperate zone. A constellation of two sensors (e.g., Landsat 5 and 7) actively acquiring data (as was the case in 2006, 2007, and 2009–2011) collects enough observations for nearly complete cloud-free coverage sufficient for annual forest change mapping and correct change date allocation. Similarly, the acquisition frequency from both Landsat 7 and 8 platforms in 2013 (Fig. 10) provides data coverage sufficient for annual monitoring until the decommissioning of Landsat 7.

4.2. Classification model performance

The approach that we present here, including the per-image calibration, per-pixel quality assessments, and time-sequential metric analyses have been developed and tested before in both regional (Hansen et al., 2008; Potapov et al., 2011, 2012) and global analyses (Hansen et al., 2013). However, the work presented here extends these prior approaches, and introduces a number of improvements. First, all reflectance and brightness temperature data were scaled to a 16-bit dynamic range, preserving radiometric resolution of the source data and enabling future Landsat 8 data incorporation. Second, the new QA models included additional input metrics such as illumination, distance to clouds, and median reflectance cloud-free reference image composite. Third, we used

Table 4
Forest cover change and annual gross forest cover loss in each country.

Country	Forest cover, (thousand ha)		Net forest cover change (% of 1985 forest)	Annual forest loss (thousand ha)			
	1985	2012		1986–1988	1989–2000	2001–2006	2007–2012
Belarus	7771	8253	6.2	30.6	37.7	48.0	44.1
Bosnia and Herzegovina	2299	2570	11.8	2.6	3.8	3.4	2.2
Bulgaria	3508	3902	11.2	9.8	6.7	12.1	9.9
Croatia	1954	2229	14.1	3.3	3.7	5.6	4.9
Czech Republic	2689	2801	4.2	13.7	10.6	17.1	27.1
Estonia	2409	2361	−2.0	7.2	11.2	22.1	26.3
Hungary	1411	1791	26.9	7.3	7.7	13.6	11.5
Kosovo	335	349	4.0	1.8	1.1	1.6	1.4
Latvia	3292	3164	−3.9	9.9	20.3	39.7	46.7
Lithuania	2008	2083	3.7	8.7	11.3	16.9	20.6
Macedonia	694	689	−0.7	2.3	1.8	3.1	3.7
Moldova	241	310	28.9	0.4	0.2	0.5	0.4
Montenegro	561	569	1.5	1.7	1.1	1.3	1.1
Poland	8470	9235	9.0	26.1	31.6	57.5	71.1
Romania	6978	7270	4.2	16.1	16.8	28.7	29.7
Russia (European Russia only)	156,996	163,289	4.0	704.4	536.6	600.5	687.2
Serbia	2246	2493	11.0	3.6	2.7	4.2	3.8
Slovakia	2176	2221	2.1	4.2	6.1	10.9	18.1
Slovenia	1214	1233	1.6	0.8	1.1	1.9	2.4
Ukraine	8671	9182	5.9	28.1	32.8	58.8	61.3

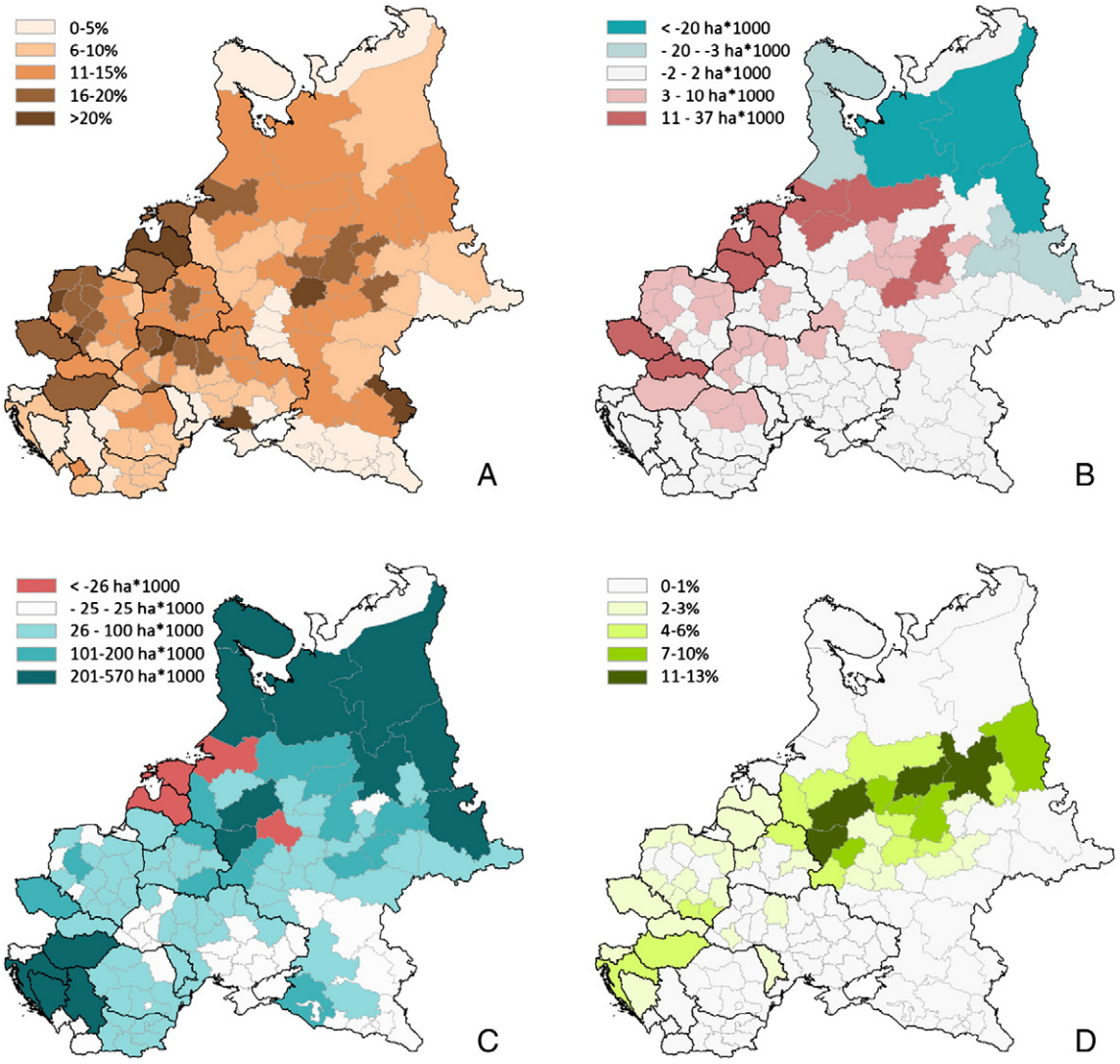

Fig. 9. Regional comparison of forest loss and forest gain: (A) forest loss 1985–2012 as percent of forest cover 1985; (B) difference (in thousand ha) of annual forest loss between 2007–2012 and 1986–1988 intervals; (C) net forest cover change between 1985 and 2012 (in thousand ha); and (D) percent of forest gain on former agricultural areas relative to the total non-forest land area in 1985.

separate QA models for different sensor types and latitude ranges to increase precision. Fourth, all QA and classification models were based on bagged classification and regression tree algorithms to improve model stability and reduce sensitivity to noise and errors in the training data. Fifth, a number of multi-temporal metrics were increased to improve class separability. Newly developed metrics included reflectance rankings based on corresponding NDVI and NDWI (which summarized spectral properties for the peak of growing season), and brightness temperature values (which, in particular, highlight spectral properties after forest cover removal). Such metrics have been employed with high temporal, low spatial resolution data sets such as MODIS, and improve the feature space when mapping land cover (Hansen et al., 2005). In addition, several complimentary time-sequential metrics were used, including the slope of the linear regression, difference between consecutive observations, and maximal difference between consecutive minimal and maximal values. Based on the forest loss classification tree model analysis, a subset of these new metrics (in addition to the first cloud-free observation reflectance and elevation) was responsible for 50% of the total deviance decrease of the tree model.

The high forest loss accuracy (Table 5) confirms the importance of QA, normalization, and metric processing approaches that we used. We compared the accuracy for 2000–2012 forest loss of our product and to the global assessment of Hansen et al. (2013) using the same reference sample data. Our product delivered user's accuracy of 94% and producer's accuracy of 88% while accuracy of global product was considerably lower, at 65% and 68%, respectively. The higher accuracy of our classification model is probably due to both a limited extent of the study area (regional vs. global) and a more sophisticated metric set with higher radiometric resolution.

The stratification aimed to target probable omission and commission errors for the forest loss validation highlighted the importance of a separate analysis for edge pixels. Because of the small patch size of many forest clearings, especially in the southern regions of the study area, the forest loss area comprised by edge pixels was larger than the area of "core" forest loss (63% and 67% of total forest loss area, respectively for 1985–2000 and 2000–2012 intervals). Errors (disagreement with reference data) were found nearly exclusively within edges (only 1 out of 67 error pixels detected for both modes was found in the "core"). Using a simple two strata design (loss/no loss) may result in an incorrect accuracy assessment, because most of the errors found within "peripheral" strata would be omitted.

The tree canopy cover mapping served an important role in the change assessment, both for mapping forest gain and for the allocation of the forest loss dates. We employed the year 2000 tree canopy cover

Table 5
Forest loss and forest gain map accuracy measures (including 95% confidence interval boundaries).

Forest loss 1985–2000	
Forest loss user's accuracy	89.9 ± 3.8
Forest loss producer's accuracy	90.0 ± 23.0
Map overall accuracy	99.6 ± 0.3
Difference between sample-based and map-based forest loss area, % of map-based estimate	−0.083 ± 0.005%
Forest loss 2000–2012	
Forest loss user's accuracy	94.3 ± 2.9
Forest loss producer's accuracy	88.2 ± 22.0
Map overall accuracy	99.6 ± 0.4
Difference between sample-based and map-based forest loss area, % of map-based estimate	+6.96 ± 0.38%
Forest gain after forest loss	
Forest gain user's accuracy	98.3 ± 1.5
Forest gain producer's accuracy	96.9 ± 1.9
Map overall accuracy	97.2 ± 1.5
Difference between sample-based and map-based forest gain area, % of map-based estimate	+1.43 ± 0.04%
Forest gain on 1985 non-forest	
Forest gain user's accuracy	91.0 ± 4.0
Forest gain producer's accuracy	75.2 ± 16.3
Map overall accuracy	98.0 ± 1.4
Difference between sample-based and map-based forest gain area, % of map-based estimate	+21.00 ± 4.58%

map produced by Hansen et al. (2013) as training data due to project limitations that precluded collecting direct training from high spatial resolution data. The resulting tree canopy cover map was used for change detection and stratification of forest cover and non-forest areas, but its accuracy is unknown. We suggest that this is not a problem because our primary goal was not to map exact values of tree canopy cover per pixel, but rather to produce a consistent time-series of tree canopy cover for change analysis. Forest gain was mapped using post-classification comparison of tree canopy cover layers, and forest loss date was attributed based on the annual tree canopy cover time-series. High accuracy of these final products, proved by our validation results, confirms the viability of our approach, and the validity of the input data that we used. Some problems remained, however. First, a post-classification method is sensitive to image misregistration especially when there are mixed pixels along forest boundaries. We solved this problem by increasing the minimum mapping unit, which, in turn, increased forest gain omission error. Second, our annual tree canopy cover model was sensitive to time of the year for available annual observations, which caused model instability in years with low image availability. Our annual forest loss allocation algorithm employed a specific set of rules to control for "spikes" in the tree canopy cover time-series.

Table 6
Field-based validation results for forest loss over abandoned agricultural areas.

Tree canopy characteristics	Total samples	Percent detected as forest gain
Height, m		
<5	26	0
5–6	22	14
7–9	19	84
>9	8	100
Tree canopy cover, %		
<10	19	0
11–30	13	8
31–50	17	18
>50	26	92
Oldest tree age, year		
<6	4	0
6–12	33	12
>12	21	81

Setting the correct tree canopy cover threshold to map the "forest cover" class is another challenge. We defined forest cover class threshold as >=49% tree canopy cover, based on a comparison with a previously published Landsat-based forest map for European Russia (Potapov et al., 2011). This threshold was used for both forest gain and "stable" forest mapping. Comparing the area of forest cover derived using this threshold for circa 2000 tree canopy cover with national forest area for year 2000 (FAO, 2010) we found that our results overestimated the area reported by FAO by only 4.07%. At the individual country level, countries with large areas of natural forests in relatively flat terrain (Poland, Estonia, Latvia, Lithuania, Slovenia) FAO reported forest areas within 10% with our forest cover estimate. However, our results overestimated forest area by 14% in countries with extensive tree plantations, and mountain areas (Romania, Bulgaria, Croatia). The same was true for the European regions of Russia when we compared our forest area with official forest cover statistics for the year 2003 (ROSLESINFORG, 2003). Our year 2000 product overestimated forest area by 4.04%, with most of the large forested regions having an official forest area estimate within 10% of our estimate. The largest difference was found in the southernmost forest-steppe and northernmost forest–tundra administrative regions, where forest cover is generally sparse. We concluded that while a forest cover map based on a consistent threshold across Eastern Europe is slightly different from national forest cover estimates, it provides a consistent measurement of established tree cover without differentiating land-use types and distinguishing trees in natural forests, plantations, and mature orchards. The forest loss product was created independently of tree canopy cover. However, our forest loss training data were consistent with our forest cover definition. Comparison of forest loss areas after 2002 with tree canopy cover 2000 showed that more than 98% of the forest loss areas had tree canopy cover of >=49% before the change event. Field verification, although limited, also confirmed our choice of the tree canopy cover threshold for the forest gain mapping. Based on these comparisons we concluded that our forest cover and forest cover loss and gain definitions were consistent between our products, and the resulting area statistics are close to national forest cover standards.

4.3. National and sub-national dynamics of forest cover

Timber harvesting is the main driver of forest cover dynamics in Eastern Europe (Schelhaas, Nabuurs, & Schuck, 2003). The extent of large natural disturbances was relatively low in our study, and comprised less than 10% of the total forest loss area. It should be noted though that we did not map small-scale, scattered disturbance, such as tree mortality due to insect infestation, as well as salvage logging, as large natural disturbance class. However, we assume that their relative extent is small. Analyzing annual forest loss (excluding large-scale fires and wind damage) per country revealed interesting parallels in forest disturbance trends (Fig. 11). Most of the countries had a small increase or decline in forest loss after the breakdown of the Soviet system in the late 1980s. However, some Central and Northern European countries more quickly transitioned to market economies, and did not decrease timber harvesting (Poland, Slovakia, Estonia, Latvia, Lithuania). Other countries experienced a pronounced decline in timber harvesting due to the economic crisis (Russia, Bulgaria, Romania) and armed conflicts (former Yugoslavia countries) in the 1990s. During the first half of the 2000s, timber harvesting increased in all countries (except Bosnia and Herzegovina). However, the global economic crisis of the late 2000s slowed down wood production in most countries, with exceptions of Central Europe and Baltic states. In many countries forest loss was lower in 2012 compared to pre-2007.

The total annual forest loss trend and the net forest cover area change within the study area was largely driven by its largest region — European Russia. Russia comprised 72% of the total forest area within the study area and was responsible for 69% of the forest loss area. Forest

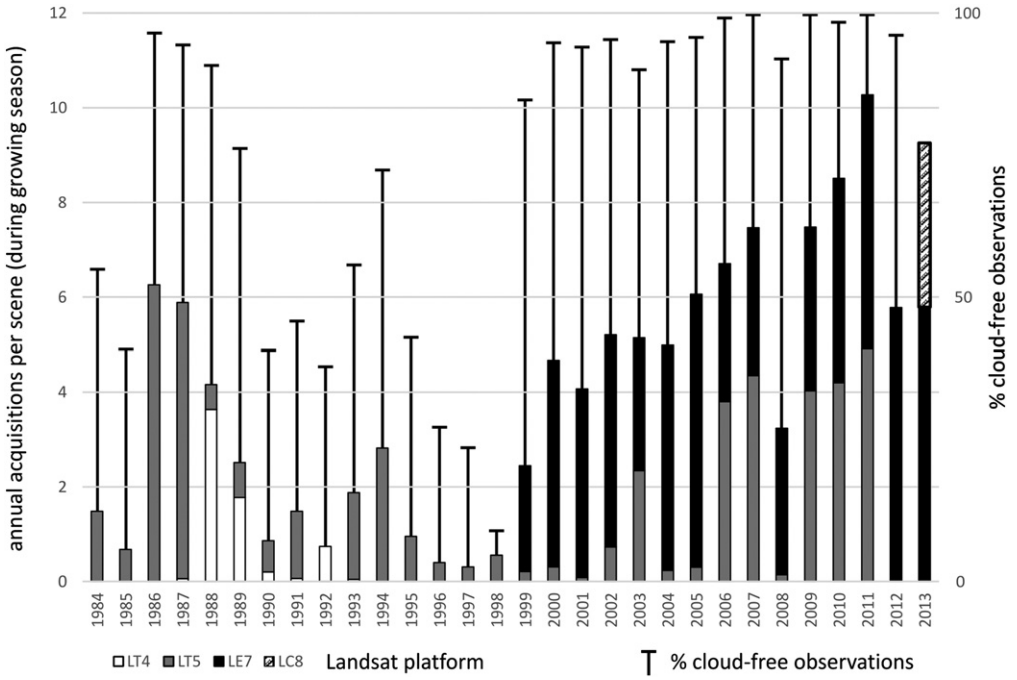

Fig. 10. Left scale: L1T image availability per sensor/year over selected 527 WRS-2 Path/Row scenes. Right scale: percent of the study area covered with annual cloud-free observations.

loss dynamic within the Russian part of the study area depended mainly on two factors: timber harvesting rates and natural disturbance events. Timber harvesting experienced dramatic changes during the transition from the Soviet planned economy to more open markets. After the breakdown of the Soviet Union, timber production decreased by 29% compared to 1990 (ROSSTAT, 2008). Since 2000 timber harvesting increased slightly, but still remained lower than in the late 1980s. This recent historical logging dynamic aligns well with our forest loss area results at the national level (Fig. 11G). Forest loss trends other than those attributed to large-scale natural disturbance in European Russia did not exhibit a statistically significant increase from 2000 to 2012.

The regional variation of forest loss and forest gain within European Russia was quite pronounced (Fig. 9). Forest loss rates (measured as percent loss of forest area) was highest in Western (especially in Leningrad) and Central regions, where it increased from the late 1980s to 2012. Logging and windfalls were responsible for the forest loss increase in the West, while wildfires of 2002 and 2010 affected Central regions. Forest loss rates in the Northern and Northeastern part were lower, and decreased even further by 2012. As a result, most of the territory experienced net forest cover gain, except the regions with the highest population density around Moscow and Saint Petersburg where extensive clearing for infrastructure and settlements occurred. Central and Northern European Russia were the hotspots for the decrease of agricultural area after the breakdown of the planned economy (Alcantara, Kuemmerle, Prishchepov, & Radeloff, 2012; Prishchepov, Radeloff, Dubinin, & Alcantara, 2012). Agricultural land abandonment and subsequent afforestation was mostly located in the southern taiga and hemiboreal forest belt, where poor soils and cold climate limit the profitability of row crop production. Cropland area within the Russian part of the study area decreased by 34% from 1990 to 2007, resulting in 28 million ha of abandoned land (ROSSTAT, 2008). According to our results, only a small fraction of these abandoned croplands (4 million ha, or 14% of total abandoned area) converted to forests, mostly due to natural succession with seed sources from nearby forests. Other areas are likely in the process of forest and shrub encroachment, but the tree canopy cover on these lands did not meet our forest cover criteria (>=49%) by year 2012. Of the total forest gain area on former agricultural lands within the study area, 64% was located in European Russia.

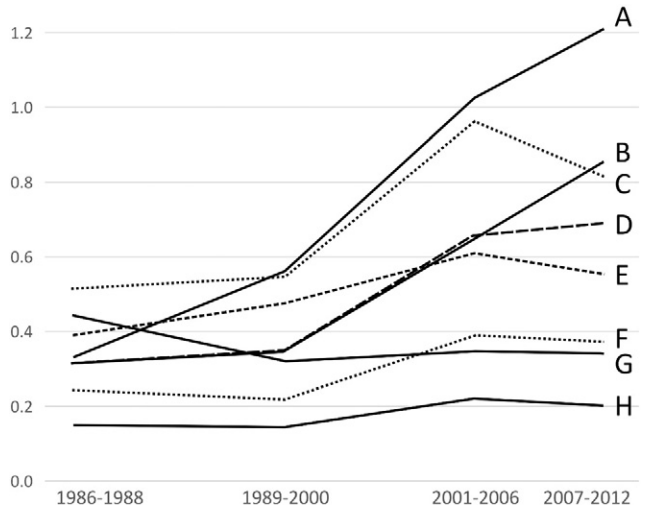

Fig. 11. Average annual gross forest cover loss (excluding wind and fire damage) as percent of year 1985 forest cover; (A) Baltic countries (Estonia, Latvia, Lithuania); (B) Central European countries (Poland, Czech Republic, Slovakia); (C) Hungary; (D) Ukraine; (E) Belarus; (F) Black sea countries (Bulgaria, Romania, Moldova); (G) European part of Russia; (H) former Yugoslavian countries (Bosnia, Croatia, Kosovo, Macedonia, Montenegro, Serbia, Slovenia).

Baltic countries represent hotspot of intensive forest use within the region. These countries are characterized by the highest disturbance rates, estimated as percent forest loss of 1985 forest cover (24% in Latvia, 22% in Lithuania, and 18% in Estonia). Most of these disturbances were due to timber harvesting. Wildfire and windstorms played a relatively small role in these countries. Forest loss within these countries did not decline during the economic transition period, and in fact experienced the highest rates of increase compared to the late 1980s (the forest loss area increase was significant with $p < 0.1e-6$ for Estonia, $p < 0.1e-7$ for Latvia, and $p < 0.001$ for Lithuania). As a result, Estonia and Latvia experienced a net forest cover decline, by 2% and 4%, respectively. Several factors may be responsible for the intensive logging and net forest cover decline: land restitution and market opening, trade liberalization after joining the European Union, short distance to paper and timber mills in Scandinavia and Poland, removal of Soviet forest

protection restrictions, and the maturing of pine plantations established immediately after World War II in areas of degraded and burned forests (Brukas, Linkevicius, & Cinga, 2009; Lazdinis, Carver, Carlsson, Tõnisson, & Vilkriste, 2004). Analysis of the relative importance of these factors will require a separate socio-economic research. The forest gain rates were also high in these countries, and young tree stands (established after 1985) comprised more than 20% of total forest cover area in Estonia and Latvia.

Overall, forest loss rates were high in Central European countries (Czech Republic, Slovakia, and Western regions of Poland). The forest loss area increased throughout the study period in Slovakia and Poland, and in Czech Republic it increased after a brief decrease in the 1990s. For all of these countries, the forest loss increase trend was statistically significant ($p < 0.001$). Interestingly, the Central European countries did not experience a decrease in timber harvesting during the economic crisis. We consider the growth of the Polish timber industry a main factor for the forest loss increase in the Central and Baltic countries. From 1985 to 2012 fiberboard production in Poland increased by a factor of 4 and paper and paperboard production doubled (FAOSTAT, http://faostat.fao.org/). As of 2012, Poland had the second largest timber processing industry in Eastern Europe (after Russia). Polish timber processing uses wood from domestic sources and from neighboring European countries. Windstorms, scattered bark beetle damage, and consequent salvage logging in mountain conifer forests contributed to forest loss in Slovakia and in Czech Republic (Seidl, Schelhaas, & Lexer, 2011). Despite high forest loss rates, forest gain dominated in these countries though resulting in net forest cover gain compared to the late 1980s.

In Hungary, forest loss increased from the late 1980s to the beginning of the 2000s, but then decreased by 25% after 2007. Hungary had the highest net increase of forest cover area (by 27%), partly due to extensive conversion of cropland to tree plantations (Griffiths et al., 2013). Because of the rapid expansion of plantations, the country had the highest percentage of young forest, i.e., forests established between 1985 and 2012 (36% of the total forest cover area) of any country in the study area.

Ukraine, Belarus, Romania, Bulgaria, and Moldova had moderate rates of forest loss, except for the Northern and Carpathians regions of Ukraine where forest logging intensity was high. Forest loss dropped in Belarus and the Black Sea countries after 2007, but remained stable in Ukraine despite the economic crisis. Our analysis showed relatively low rates of afforestation on former agriculture lands in these countries, with the exception of substantial forest gain on former cropland areas in Northern Belarus and around the Chernobyl Exclusion Zone in Ukraine. In Belarus, the stability of agricultural land is partly due to governmental subsidies and regulations (World Bank, 2009). All these countries experienced small net forest cover area increase.

Former Yugoslavian countries were characterized by relatively low forest loss rates. Slovenia and Macedonia had only a small increase of annual forest loss area since the 1990s. Fore loss rates in all other countries dropped after 2007, and in Bosnia and Herzegovina after 2000. Wildfire plays an important role in forest loss in Macedonia, Montenegro, Croatia, and Bosnia, especially during extreme fire years of 2000 and 2007 (European Commission, 2011; Nikolov, 2006). According to our data, wildfires comprised 8–15% of the total forest loss within these countries. Extensive forest gain, including forest regrowth on abandoned croplands and pastures, caused net forest cover to increase by more than 10% relative to 1985's forest cover in Bosnia, Croatia, and Serbia. Due to the economic crisis and population displacement after armed conflicts in the 1990s, entire settlements and all surrounding cropland areas were abandoned in Croatia and Bosnia, and there was widespread tree encroachment in these locations (Witmer, 2008). Because of their low forest disturbance rates, Slovenia and Montenegro had the largest proportion of mature forest stands (established before 1985) of total forest cover compared to other countries within the study area.

While the fraction of large-scale natural disturbance (windstorms and wildfires) was low, the extent and frequency of these disturbance events did increase in the 2000s compared to 1985–1999. Large-scale natural disturbances played an increasingly important role in European Russia compared to other countries. Wildfire was responsible for 8.1% of the forest loss area in European Russia, compared to 1.8% outside of this region, and windstorms were responsible for 1.6% in European Russia, compared to 0.7% outside. The role of natural disturbance increased throughout the analyzed time interval. The percentage of wildfire changed from 1.5% in 1986–1988 to 11.3% in 2007–2012 (annual trend statistically significant with $p < 0.01$). Windstorms were responsible for less than 1% of the forest loss until 2006, but up to 3.6% in 2007–2012 (trend statistically significant with $p < 0.001$). Both types of natural disturbance are more common during extreme weather conditions. The drought and windstorm frequency increased after 2000, which may be related to the overall temperature increase and global climate warming (Schelhaas et al., 2003; Seidl et al., 2011; Groisman & Soja, 2009), but past forest management, especially the planting of spruce monocultures that are more susceptible to windthrow may have also exacerbated the effects of these storms. Extensive windstorms affected the Czech Republic in the 1990s (Jizera Mountains); Slovakia in 2004 (Tatra Mountains); and European Russia in 2009 (Kirov and Komi regions) and in 2010 (Leningrad, Novgorod, Yaroslavl, Vologda regions) (Krylov, Malahova, & Vladimirova, 2012). Mediterranean forests in the former Yugoslavia experienced fires predominantly during the 1990s. In European Russia extreme fire events occurred in 1997 and 1999 (West and Northwestern regions), 2000 (Northern regions), 2002, and 2010 (Central regions). The forest loss area caused by European Russia fires did affect the total fire-related annual forest loss trend within the study area (Fig. 7). However, we stress that we mapped only large-scale wind and fire damage. Smaller-scale burned areas, windfalls, and forest dieback due to insect infestation were not mapped. Mapping small-scale scattered disturbance type is a complicated task and should be addressed in future research.

While most of the forest disturbance within the study area quickly recovered, certain portions of forest loss had no signs of tree cover gain (Fig. 8). For example, of the forest loss area that occurred between 1985 and 1995 almost 12% did not recover by 2005. There are two likely causes for this. Some of these areas may represent permanent land-cover conversion where forests were replaced by either settlements or infrastructure. Other areas, especially in the northern boreal forests or in dry climate, may represent slow forest regeneration.

5. Conclusion

Our analysis proved the feasibility of a Landsat-based, long-term (27 years) forest cover change assessment for a large region. Despite data limitations, especially the incomplete Landsat archive for the 1990s, our proposed approach for the mapping of gross forest cover loss and gain events was successful and enabled the estimation of net forest cover change. Our validation, which was performed using probability-based sampling and specifically focused on classification errors within edge pixels, showed high quality of the developed map products. Results can easily be aggregated from 30-m pixels to various national and sub-national units to perform regional forest cover and change analyses.

Our results at the national scale confirmed the forest cover increase reported by FAO (2010). However, regional analysis showed substantial variation of forest cover change, especially within large countries. Areas with net forest cover loss, especially Estonia, Latvia, Saint Petersburg and Moscow regions of Russia, are of concern as they may represent examples of unsustainable forest use. The effect of recent socio-economic changes, including the collapse of the planned economies, armed conflicts in Balkan countries, changes in agriculture policy after EU expansion, and the economic crisis of late 2000s, clearly manifested themselves in our forest change data. The role of large-scale natural disturbance and their increase in the recent decade was also notable. Our results provide a baseline for further socio-economic research to select dominant factors regulating forest cover changes at national and sub-

national level. Providing our results as independent, consistent data source for unrestricted use (http://glad.geog.umd.edu/europe/) enables such analyses.

The constellation of multiple Landsat satellites (L5/L7 in mid-2000s) allowed for nearly-complete annual cloud-free data coverage in some years. While the existing constellation of L7/L8 is sufficient for such analyses, single sensor constellations, e.g., a sole L8 after the decommissioning of L7, will not be sufficient for annual data collection in our study area given the short growing season and frequent cloud cover. Other solutions such as the integration of L8 with the future Sentinel missions, and the launch of a follow-on Landsat 9 sensor, are needed to fill this looming data gap.

Acknowledgements

The project was supported by NASA Land-Cover/Land-Use Change Program research grants NNX13AC66G and NNX12AG74G. We greatly appreciate help in fieldwork from our colleagues E. Boren, M. Doktorova, M. Dubinin, A. Manisha, and A. Purekhovsky; and valuable comments by Dr. L. Laestadius and two anonymous reviewers.

References

Alcantara, C., Kuemmerle, T., Prishchepov, A.V., & Radeloff, V.C. (2012). Mapping abandoned agriculture with multi-temporal MODIS satellite data. *Remote Sensing of Environment*, *124*, 334–347.

Baumann, M., Ozdogan, M., Kuemmerle, T., Wendland, K.J., Esipova, E., & Radeloff, V.C. (2012). Using the Landsat record to detect forest-cover changes during and after the collapse of the Soviet Union in the temperate zone of European Russia. *Remote Sensing of Environment*, *124*, 174–184.

Breiman, L. (1996). Bagging predictors. *Machine Learning*, *24*, 123–140.

Breiman, L., Friedman, J.H., Olshen, R.A., & Stone, C.J. (1984). *Classification and regression trees*. Monterey, California: Wadsworth and Brooks/Cole.

Broich, M., Hansen, M.C., Potapov, P., Adusei, B., Lindquist, E., & Stehman, S.V. (2011). Time-series analysis of multi-resolution optical imagery for quantifying forest cover loss in Sumatra and Kalimantan, Indonesia. *International Journal of Applied Earth Observation and Geoinformation*, *13*(2), 277–291.

Brukas, V., Linkevicius, E., & Cinga, G. (2009). Policy drivers behind forest utilisation in Lithuania in 1986–2007. *Baltic Forestry*, *15*(1), 86–96.

Burgess, R., Hansen, M., Olken, B.A., Potapov, P., & Sieber, S. (2012). The political economy of deforestation in the tropics. *Quarterly Journal of Economics*, *127*(4), 1707–1754.

Carroll, M., Townshend, J.R.G., Hansen, M.C., DiMiceli, C., Sohlberg, R., & Wurster, K. (2010). Vegetative cover conversion and vegetation continuous fields. In B. Ramachandran, C. Justice, & M. Abrams (Eds.), *Land remote sensing and global environmental change: NASA's EOS and the science of ASTER and MODIS*. New York: Springer.

Chander, G., Markham, B.L., & Helder, D.L. (2009). Summary of current radiometric calibration coefficients for Landsat MSS, TM, ETM+, and EO-1 ALI sensors. *Remote Sensing of Environment*, *113*, 893–903.

Cohen, W.B., Yang, Z., & Kennedy, R. (2010). Detecting trends in forest disturbance and recovery using yearly Landsat time series: 2. TimeSync — Tools for calibration and validation. *Remote Sensing of Environment*, *114*, 2911–2924.

Danielson, J.J., & Gesch, D.B. (2011). Global multi-resolution terrain elevation data 2010 (GMTED2010): U.S. Geological Survey. *Open-File Report 2011-1073*.

DeFries, R., Hansen, M., & Townshend, J. (1995). Global discrimination of land cover types from metrics derived from AVHRR Pathfinder data. *Remote Sensing of Environment*, *54*, 209–222.

DeFries, R.S., Houghton, R.A., Hansen, M.C., Field, C.B., Skole, D., & Townshend, J. (2002). Carbon emissions from tropical deforestation and regrowth based on satellite observations for the 1980s and 1990s. *Proceedings of the National Academy of Sciences*, *99*(22), 14256–14261.

Eliasson, P. (2002). *Skog, makt och människor. En miljöhistoria om svensk skog 1800–1875 [Forest, power and people. An environmental history of Swedish forest 1800–1875]*. Stockholm: KSLA (453 pp. [in Swedish]).

European Commission (2011). *Forest fires in Europe 2010 (EUR 24910 EN)*. Luxembourg: Publication Office of the European Union.

European Environment Agency (2007). *CORINE Landcover 2006 technical guidelines*. Luxembourg: Office for Official Publications of the European Communities (DOI 10.2800/12134).

FAO [Food and agriculture organization of the United Nations] (2010). *Global forest resources assessment 2010*. Rome: UNFAO.

Fuchs, R., Herold, M., Verburg, P.H., & Clevers, J.G.P.W. (2013). A high-resolution and harmonized model approach for reconstructing and analyzing historic land changes in Europe. *Biogeosciences*, *10*, 1543–1559.

Gallaun, H., Zanchi, G., Nabuurs, G. -J., Hengeveld, G., Schardt, M., & Verkerk, P.J. (2010). EU-wide maps of growing stock and above-ground biomass in forests based on remote sensing and field measurements. *Forest Ecology and Management*, *260*(3), 252–261.

Gao, B. (1996). NDWI — A normalized difference water index for remote sensing of vegetation liquid water from space. *Remote Sensing of Environment*, *58*(3), 257–266.

Griffiths, P., Kuemmerle, T., Kennedy, R.E., Abrudan, I.A., Knorn, J., & Hostert, P. (2012). Using annual time-series of Landsat images to assess the effects of forest restitution in post-socialist Romania. *Remote Sensing of Environment*, *118*, 199–214.

Griffiths, P., Muller, D., Kuemmerle, T., & Hostert, P. (2013). Agricultural land change in the Carpathian ecoregion after the breakdown of socialism and expansion of the European Union. *Environmental Research Letters*, *8*, 045024.

Groisman, P.Y., & Soja, A. (2009). Ongoing climatic change in Northern Eurasia: Justification for expedient research. *Environmental Research Letters*, *4*, http://dx.doi.org/10.1088/1748-9326/4/4/045002.

Hansen, M.C., Potapov, P.V., Moore, R., Hancher, M., Turubanova, S.A., Tyukavina, A., et al. (2013). High-resolution global maps of 21st-century forest cover change. *Science*, *342*(6160), 850–853.

Hansen, M.C., Roy, D.P., Lindquist, E., Adusei, B., Justice, C.O., & Altstatt, A. (2008). A method for integrating MODIS and Landsat data for systematic monitoring of forest cover and change and preliminary results for Central Africa. *Remote Sensing of Environment*, *112*, 2495–2513.

Hansen, M.C., Townshend, J.R.G., DeFries, R.S., & Carroll, M. (2005). Estimation of tree cover using MODIS data at global, continental and regional/local scales. *International Journal of Remote Sensing*, *26*, 4359–4380.

Harris, N.L., Brown, S., Hagen, S.C., Saatchi, S.S., Petrova, S., Salas, W., et al. (2012). Baseline map of carbon emissions from deforestation in tropical regions. *Science*, *336*(6088), 1573–1576.

Johann, E. (2004). Forest history in Europe. In D. Werner (Ed.), *Biological resources and migration* (pp. 73–82). Berlin: Springer.

Kalyakin, V.N., Smirnova, O.V., Bobrovskii, M.V., Turubanova, S.A., Potapov, P.V., & Yaroshenko, A.Y. (2004). History of the Eastern European forest cover. In O.V. Smirnova (Ed.), *Forests of Eastern Europe* (pp. 51–153). Moscow, Russia: Nauka ([in Russian]).

Kaplan, J.O., Krumhardt, K.M., & Zimmermann, N. (2009). The prehistoric and preindustrial deforestation of Europe. *Quaternary Science Reviews*, *28*, 3016–3034.

Kaplan, J.O., Krumhardt, K.M., & Zimmermann, N.E. (2012). The effects of land use and climate change on the carbon cycle of Europe over the past 500 years. *Global Change Biology*, *18*, 902–914.

Krylov, A.M., Malahova, E.G., & Vladimirova, N.A. (2012). Identification and assessment of forest areas damaged by windfalls in 2009–2010 by means of remote sensing. *Izvestija Sankt-Peterburgskoj lesotehnicheskoj akademii. 200*. (pp. 197–207) ([in Russian]).

Kuemmerle, T., Chaskovskyy, O., Knorn, J., Radeloff, V.C., Kruhlov, I., Keeton, W.S., et al. (2009). Forest cover change and illegal logging in the Ukrainian Carpathians in the transition period from 1988 to 2007. *Remote Sensing of Environment*, *113*(6), 1194–1207.

Kuemmerle, T., Hostert, P., Radeloff, V.C., Perzanowski, K., & Kruhlov, I. (2007). Postsocialist forest disturbance in the Carpathian border region of Poland, Slovakia, and Ukraine. *Ecological Applications*, *17*, 1279–1295.

Kuemmerle, T., Radeloff, V.C., Perzanowski, K., & Hostert, P. (2006). Cross-border comparison of land cover and landscape pattern in Eastern Europe using a hybrid classification technique. *Remote Sensing of Environment*, *103*, 449–464.

Lazdinis, M., Carver, A., Carlsson, L., Tõnisson, K., & Vilkriste, L. (2004). Forest policy networks in changing political systems: Case study of the Baltic states. *Journal of Baltic Studies*, *35*(4), 402–419, http://dx.doi.org/10.1080/01629770400000181.

Margono, B.A., Turubanova, S., Zhuravleva, I., Potapov, P., Tyukavina, A., Baccini, A., et al. (2012). Mapping and monitoring deforestation and forest degradation in Sumatra (Indonesia) using Landsat time series datasets from 1990 to 2010. *Environmental Research Letters*, *7*(3), http://dx.doi.org/10.1088/1748-9326/7/3/034010.

Morse, V. (2007). The role of maps in later medieval society: Twelfth to fourteenth century. In D. Woodward (Ed.), *Cartography in the European renaissance. In: Vol. 3 of the history of cartography* (pp. 25–52). Chicago: University of Chicago Press.

Nikolov, N. (2006). Global forest resources assessment 2005 — Thematic report on forest fires in the Balkan Region. *FAO Fire Management Working Paper #11*. Rome: FAO.

Olofsson, P., Foody, G.M., Herold, M., Stehman, S.V., Woodcock, C.E., & Wulder, M.A. (2014). Good practices for estimating area and assessing accuracy of land change. *Remote Sensing of Environment*, *148*, 42–57.

Pekkarinen, A., Reithmaier, L., & Strobl, P. (2009). Pan-European forest/non-forest mapping with Landsat ETM+ and CORINE Land Cover 2000 data. *ISPRS Journal of Photogrammetry and Remote Sensing*, *64*, 171–183.

Pflugmacher, D., Cohen, W.B., & Kennedy, R.E. (2012). Using Landsat-derived disturbance history (1972–2010) to predict current forest structure. *Remote Sensing of Environment*, *122*, 146–165.

Pflugmacher, D., Cohen, W.B., Kennedy, R.E., & Yang, Z. (2014). Using Landsat-derived disturbance and recovery history and lidar to map forest biomass dynamics. *Remote Sensing of Environment*, *151*, 124–137.

Potapov, P., Turubanova, S., & Hansen, M.C. (2011). Regional-scale boreal forest cover and change mapping using Landsat data composites for European Russia. *Remote Sensing of Environment*, *115*, 548–561.

Potapov, P.V., Turubanova, S.A., Hansen, M.C., Adusei, B., Broich, M., Altstatt, A., et al. (2012). Quantifying forest cover loss in Democratic Republic of the Congo, 2000–2010, with Landsat ETM+ data. *Remote Sensing of Environment*, *122*, 106–116.

Prishchepov, A.V., Radeloff, V.C., Dubinin, M., & Alcantara, C. (2012). The effect of Landsat ETM/ETM + image acquisition dates on the detection of agricultural land abandonment in Eastern Europe. *Remote Sensing of Environment*, *126*, 195–209.

Reed, B.C., Brown, J.F., VanderZee, D., Loveland, T.R., Merchant, J.W., & Ohlen, D.O. (1994). Measuring phenological variability from satellite imagery. *Journal of Vegetation Science*, *5*, 703–714.

Richter, R. (2010). *Atmospheric/topographic correction for satellite imagery — ATCOR2/3 user guide*. DLR — German Aerospace Center.

ROSLESINFORG (2003). *Forest fund of Russia (data of state forest account)*. Moscow: VNIILM ([in Russian]).
ROSSTAT [Russian Federal State Statistics Service] (2008). *Regions of Russia: Social and economic indicators*. Russia: Moscow ([in Russian]).
Schelhaas, M.J., Nabuurs, G.J., & Schuck, A. (2003). Natural disturbances in the European forests in the 19th and 20th centuries. *Global Change Biology*, *9*(11), 1620–1633.
Schuck, A., Päivinen, R., Häme, T., Van Brusselen, J., Kennedy, P., & Folving, S. (2003). Compilation of a European forest map from Portugal to the Ural mountains based on earth observation data and forest statistics. *Forest Policy and Economics*, *5*(2), 187–202.
Seebach, L., Strobl, P., San Miguel-Ayanz, J., Gallego, J., & Bastrup-Birk, A. (2011). Comparative analysis of harmonized forest area estimates for European countries. *Forestry*, *84*, 285–299.
Seidl, R., Schelhaas, M.J., & Lexer, M.J. (2011). Unraveling the drivers of intensifying forest disturbance regimes in Europe. *Global Change Biology*, *17*(9), 2842–2852.
Stehman, S.V. (2012). Impact of sample size allocation when using stratified random sampling to estimate accuracy and area of land-cover change. *Remote Sensing Letters*, *3*, 111–120.
Stehman, S.V. (2013). Estimating area from an accuracy assessment error matrix. *Remote Sensing of Environment*, *132*, 202–211.
Stehman, S.V., & Czaplewski, R.L. (1998). Design and analysis of thematic map accuracy assessment: Fundamental principles. *Remote Sensing of Environment*, *64*, 331–344.
Tomppo, E., Gschwantner, Th., Lawrence, M., & McRoberts, R.E. (2010). *National forest inventories*. New York: Springer (DOI 10.1007/978-90-481-3233-1).
Tyukavina, A., Stehman, S.V., Potapov, P.V., Turubanova, S.A., Baccini, A., Goetz, S.J., et al. (2013). National-scale estimation of gross forest aboveground carbon loss: A case study of the Democratic Republic of the Congo. *Environmental Research Letters*, *8*(4), http://dx.doi.org/10.1088/1748-9326/8/4/044039.
Vermote, E.F., Saleous, N.Z., & Justice, C.O. (2002). Atmospheric correction of MODIS data in the visible to middle infrared: first results. *Remote Sensing of Environment*, *83*, 97–111.
Wendland, K.J., Lewis, D.J., Alix-Garcia, J., Ozdogan, M., Baumann, M., & Radeloff, V.C. (2011). Regional- and district-level drivers of timber harvesting in European Russia after the collapse of the Soviet Union. *Global Environmental Change*, *21*(4), 1290–1300.
Witmer, F.D.W. (2008). Detecting war-induced abandoned agricultural land in northeast Bosnia using multispectral, multitemporal Landsat TM imagery. *International Journal of Remote Sensing*, *29*, 3805–3831.
World Bank (2009). Belarus: agricultural productivity and competitiveness. Impact of state support and market intervention. *Report No. 48335-BY* ([http://siteresources.worldbank.org/INTBELARUS/Resources/PDF_DOC.pdf]).